Comparative analysis of amine-functionalized silica for direct air capture (DAC): Material characterization, performance, and thermodynamic efficiency

Riham Surkatti, Yasser M. Abdullatif, Raeesh Muhammad, Ahmed Sodiq, Kamal Mroue, Tareq Al-Ansari, Abdulkarem I. Amhamed

Separation and Purification Technology 354 (2025) 128641

Contents lists available at ScienceDirect

Separation and Purification Technology

journal homepage: www.elsevier.com/locate/seppur

Comparative analysis of amine-functionalized silica for direct air capture (DAC): Material characterization, performance, and thermodynamic efficiency

Riham Surkatti [a], Yasser M. Abdullatif [a,b], Raeesh Muhammad [a], Ahmed Sodiq [a], Kamal Mroue [c], Tareq Al-Ansari [a,b], Abdulkarem I. Amhamed [a,*]

[a] Qatar Environment and Energy Research Institute (QEERI), Hamad Bin Khalifa University, Qatar Foundation, Education City, Doha, Qatar
[b] College of Science and Engineering, Hamad Bin Khalifa University, Qatar Foundation, Doha, Qatar
[c] Core Laboratories, Hamad Bin Khalifa University, Qatar Foundation, Education City, Doha, Qatar

ARTICLE INFO

Editor: S. Deng

Keywords:
DAC
Kinetic models
SBA-15
Indoor conditions
Thermodynamic efficiency

ABSTRACT

Direct air capture (DAC) technology faces challenges due to energy-intensive processes and limited CO_2 capture capacity under atmospheric concentration. Utilizing adsorption techniques with solid sorbents offers a sustainable solution. This study investigates the performance, efficiency, and regeneration energy of various amines (TEPA, low and high molecular weights PEI and APTES) functionalized mesoporous silica (SBA-15) for DAC. Comprehensive investigations, including characterization and thermodynamic efficiency evaluation, are conducted for CO_2 adsorption under dry and humid conditions (50 % RH). Functionalizing SBA-15 with TEPA, PEI-L and PEI-H, and TEPA significantly improves CO_2 adsorption, increasing capacities to 2.1, 1.36, and 1.11 mmol/g, respectively, and introduction of humidity further increases CO_2 capacities to 3.17, 2.87, and 1.68 mmol/g, respectively. However, there's a trade-off in thermodynamic efficiency due to energy consumed in desorbing water molecules. S-TEP exhibits the highest thermodynamic efficiency in dry conditions, while S-PEI-L achieves the highest efficiency in humid conditions. Stability tests of all material in addition to, the commercial material, lewatit demonstrate robust regenerability over 10 cycles under both dry and humid conditions (50 % RH). This study provides insights into functionalized SBA-15 performance in CO_2 adsorption, with implications for efficient and sustainable indoor DAC processes.

1. Introduction

The surge in atmospheric concentration of carbon dioxide (CO_2), driven by anthropogenic emissions, stands as a singular threat to global stability and sustainable development, largely impacting marginalized populations worldwide [1–3]. The extent of this crisis, characterized by almost 36.3 gigaton/year of global CO_2 emissions, demands urgent action from nations across the globe to achieve net-zero CO_2 emissions by 2050, as recommended by the Intergovernmental Panel on Climate Change (IPCC) [4,5]. This ambitious target necessitates a multifaceted approach that encompasses both CO_2 removal and carbon emission reduction strategies [6]. Direct air capture (DAC), a technology that extracts CO_2 directly from ambient air, has emerged as a critical tool to complement carbon capture from concentrated sources like flue gas [7]. The concept of DAC was initially introduced by Lackner nearly two decades ago [8], but progress in commercialization in this area has been slow largely due to the high energy required to capture CO_2 and to regenerate the sorbents. The current DAC systems primarily rely on sorption techniques using solid sorbents, which consume less energy only by using the waste heat when compared to liquid-based absorption techniques [9,10]. However, the extremely diluted concentration of CO_2 in the atmosphere, around 400 ppm by volume, poses a substantial challenge in capturing CO_2 using solid sorbents. This limitation restricts the CO_2 sorption capacity of these sorbents to a range of 1.0 to 1.5 mol/kg [11,12]. Moreover, almost all researched sorbents thus far, including organic–inorganic hybrids, polyethyleneimines, polyamines, metal–organic frameworks and anion exchange resins, require thermal energy for desorption [13,14]. Previous studies have highlighted the significant energy efficiency and economic benefits of DAC systems that utilize sorbents with high sorption capacities and efficient regeneration

* Corresponding author.
E-mail address: aamhamed@hbku.edu.qa (A.I. Amhamed).

https://doi.org/10.1016/j.seppur.2024.128641
Received 6 April 2024; Received in revised form 26 June 2024; Accepted 29 June 2024
Available online 8 July 2024

processes[15,16]. Therefore, developing high-capacity CO_2 capture materials under ambient conditions is of paramount importance to ensure the timely implementation of DAC systems and achieve the IPCC's 2050 target.

Mesoporous silica materials are gaining growing interest as a significant category of nanostructured support materials in carbon capture [17], especially in direct air capture [18]. Their substantial surface area, precisely defined porous structure, and capacity to integrate metal atoms within the mesopores make them a promising choice for various adsorbent designs [19]. Specifically, the SBA-15 mesoporous silica stands out due to its versatile applications in direct air capture of CO_2, attributed to its thicker walls that result in enhanced thermal and mechanical stability [20]. While previous research has demonstrated significant advances in CO_2 capture capacity using amine-functionalized SBA-15[21], reaching up to 5 mmol/g [22], these studies often neglect a crucial aspect – the impact of atmospheric humidity. The presence of water vapor significantly influences CO_2 adsorption dynamics, often resulting in trade-offs between capacity and regeneration energy. Furthermore, the cost-effectiveness of such materials remains a critical consideration for DAC implementation. There have been previous research activities on amine functionalized SBA-15 involving high-molecular-weight PEI (PEI-H) [23] and low molecular weight PEI (PEI-L) [19,24]. For the PEI-H, the study demonstrated promising CO_2 capture capacities with PEI-H functionalized SBA-15 but for flue gas applications. For the low-molecular-weight PEI (PEI-L), literature is replete with several PEI-L functionalized SBA-15 for DAC applications. The reason for this can be found in the work of Meng et al. [25], which reported that adsorbents with higher PEI loadings (45–55 %) and high molecular weight (Mw ca. 1200–25,000) exhibited superior CO_2 capture performance. These materials provided the necessary binding affinity for efficient CO_2 capture even at elevated temperatures, which is more suitable for applications like flue gas capture. Adsorbents with moderate PEI loading (30–40 %) and medium molecular weight (Mw ca. 600–800) demonstrated optimal performance. These materials offered a balance between CO_2 capture and desorption, making them suitable for applications like direct air capture biogas upgrading. However, careful temperature control during desorption is crucial to avoid premature CO_2 release. Despite lower capacities, PEI-L often requires lower regeneration temperatures due to weaker CO_2 binding. This can offer potential advantages in terms of energy consumption and thermodynamic efficiency. Tetraethylenepentamine (TEPA) is a promising amine for CO_2 capture due to its comparable CO_2 uptake capacity in post-combustion applications [26]. However, TEPA's low boiling point and volatility compromise its stability for DAC, leading to narrow operating temperature range [27]. TEPA-modified adsorbents perform poorly outside of a specific temperature range, hindering their viability for ambient temperatures in DAC. Consequently, TEPA-modified mesoporous molecular sieve composites have not been extensively studied for DAC applications [19].

For direct air capture and humidity, for different sorbents, water acts as both an inhibitor and promoter of CO_2 adsorption [28]. Understanding these multi-faceted roles is crucial for optimizing capture performance. In DAC, co-adsorbed water creates a complex system that requires careful consideration [28]. Unlike conventional sorbents, water is essential for the long-term stability of amine-based materials, adding another layer of complexity to their design and operation. Designing effective CO_2 capture technologies necessitates a deep understanding of how water interacts with specific sorbents and processes. Controlling moisture levels and their influence on sorption kinetics becomes crucial for optimal performance, particularly in DAC systems. Tailoring amine-based sorbents to mitigate water's negative effects while utilizing its stabilizing properties requires further research and development. While some studies report decreased CO_2 adsorption capacity with moisture (competitive adsorption), others highlight positive effects like increased capture rate or acting as a co-adsorbent (facilitating capture) [29]. Under dry conditions, co-adsorbed water can significantly increase the energy needed for sorbent regeneration (up to several folds) due to its higher heat of desorption [30]. Implementing heat recovery strategies can minimize the water associated energy penalty [30].

Considering the above, the present study addresses these knowledge gaps by comprehensively investigating the impact of various amine functionalization groups on CO_2 adsorption performance in the context of DAC. We systematically assess the CO_2 capture capacities of SBA-15 functionalized with polyethylenimines (PEIs) of different molecular weights, tetraethylenepentamine (TEPA), and amino-propyltriethoxysilane (APTES) under both dry and humid conditions. Furthermore, we delve into the crucial aspect of regeneration energy requirements, calculating the thermodynamic efficiency and assessing the effect of cyclic stability of each material. Our findings unveil a nuanced picture of the interplay between functionalization, CO_2 adsorption, and thermodynamic efficiency. While certain amines like PEI-L, PEI-H, and TEPA significantly enhance CO_2 uptake compared to unmodified SBA-15, exceeding 3 mmol/g even in humid conditions, the presence of water vapor introduces energy challenges during regeneration. This trade-off underscores the importance of considering not just capacity, but also energy efficiency and cost when designing adsorbents for practical DAC applications. Despite these challenges, our research identifies promising materials for future DAC development that can be used in indoor DAC with RH of 50 %. S-TEPA demonstrates the highest thermodynamic efficiency in dry conditions, while S-PEI-H exhibits the most efficient performance in humid environments. These findings pave the way for the rational design of next-generation adsorbents tailored for specific DAC operating conditions, balancing capacity, efficiency, and cost-effectiveness.

2. Materials and methods

All chemicals and materials are commercially available and were used without any further processing/purification unless otherwise mentioned. Mesoporous Silica (SBA-15), TEPA, branched polyethyleneimine low molecular weight (M_w ca. 800) (PEI-L), high molecular weight (M_w ca. 25000) (PEI-H), APTES, methanol and hexane were procured from Sigma- Aldrich.

2.1. Adsorbent development

The functionalization of SBA-15 using PEI-L, PEI-H and TEPA was performed through the wet impregnation method, to develop three different amine-based adsorbents. In a typical impregnation reaction, SBA-15 (1.0 g) was dispersed in methanol (20 ml) by stirring. Separately amine precursors (1.0 g) were dissolved in methanol (10 ml). The amine precursor solutions were then added to the silica dispersion with continuous stirring, and further stirred for three hours at room temperature (298 K). The functionalized products were obtained by removing the solvent using rotary evaporator (for PEI-L and PEI-H functionalized materials), and normal heating at 50 °C (for TEPA functionalized material). Furthermore, the functionalization of SBA-15 with APTES was achieved through chemical grafting, in which SBA-15 (1 g) was dispersed in n-hexane (35 ml) and to this APTES (1 g) dissolved in n-hexane (15 ml) was added dropwise and refluxed for 12 h at 80 °C and then allowed to cool naturally. The product was separated by centrifugation and washed with n-hexane. Thus, the obtained SBA-15 materials functionalized with PEI-L, PEI-H, TEPA and APTES were designated as S-PEI-L, S-PEI-H, S-TEP and S-APT, respectively.

2.2. Adsorbent characterization

Fourier Transform Infrared (FT-IR) measurements were carried out in transmittance mode on a Thermo Scientific Nicolet iS50 FT-IR spectrometer equipped with an attenuated total reflectance (ATR) sampling accessory with a diamond crystal plate. Spectra were recorded with 32 scans per sample/background in the spectral range of 4000 – 400 cm^{-1}

at 4 cm^{-1} spectral resolution. Thermal gravimetric analysis (TGA) was performed on Universal V4.5A TA Instruments under N_2 atmosphere in the temperature range from room temperature (RT, 25 °C) to 800 °C with a heating rate of 10 °C/minute. Microstructural images were recorded on Quanta650FEG Fourier emission scanning electron microscopy (FE-SEM). Elemental analysis was carried out using X-ray photon spectroscopy (XPS, Thermo Fisher ESCALAB 250XI) and electron dispersive X-ray spectroscopy (EDS, Bruker Quantax400). The porosity before and after functionalization was accessed by measuring the N_2 sorption analysis at 77 K, and CO_2 uptake at RT using ASAP 2420 (Micromeritics) after degassing the sample under dynamic vacuum at 90 °C for 12 h. Specific surface area (SSA) was estimated using the Brunauer–Emmett–Teller (BET) model, and total pore volume was calculated at $P/P_0 = 0.99$ (adsorption branch).

2.3. Adsorption experiments

A laboratory setup has been established to evaluate the dynamic capturing process under atmospheric conditions with a CO_2 concentration of 420 ppm. The setup consists of three main components: gases, adsorption/regeneration, and monitoring. The gases section includes gas cylinders containing nitrogen, CO_2 and dry air. The adsorption/regeneration section features a cooling/heating jacket and humidifier to control the adsorption temperature and humidity, a reactor for loading the sample, and a heating element for regeneration. The third section includes a micro-GC, which allows for the measurement of CO_2 uptake by the materials, the breakthrough curve, CO_2 recovery, and the purity of gas streams. Additionally, measuring devices for mass flow rate, temperature, humidity, and pressure drop through the reactor are installed to enable the real-time monitoring of key parameters, as shown in Fig. 1.

The adsorption experiments in this study involved the utilization of a 0.2 g sample of the material installed in a reactor supported by quartz wool. The DAC cycle conducted here comprised four distinct steps. Firstly, the material underwent degassing by heating to 90 °C, followed by purging with a pure N_2 flow at a rate of 60 ml/min. This process continued until the Gas Chromatography (GC) indicated that only N_2 was emanating from the reactor, ensuring thorough degassing. In the second stage, adsorption commenced with the introduction of air from the atmosphere with a flow rate of 35 ml/min. Prior to initiating the adsorption experiments, the actual air composition was determined using GC, revealing 420 ppm CO_2, 78.9 % N_2, 21 % O_2, and about 1 % argon. To maintain dry experimental conditions, silica gel was employed to capture water content. The silica gel's saturation with CO_2 was verified using GC before the adsorption tests began. For humid experiments, a device was employed to humidify the air to 50 % relative humidity (RH), in which the RH is the typical value for the indoor application. The adsorption experiments concluded when the concentration of CO_2 in the reactor outlet air reached 420 ppm. The third stage involved regenerating the adsorbent by heating it to 90 °C, purging with N_2, and quantifying the regenerated CO_2 and water. The fourth stage included cooling the adsorbent to prepare it for a new DAC cycle. This comprehensive methodology ensured a systematic and controlled approach to testing the adsorbents in the DAC cycle.

2.4. Regeneration energy and efficiency calculation

The energy requirements for a TVSA process are estimated based on the work reported in reference [31]. Factors considered include the vacuum pump work of desorbed CO_2, the heat of desorption of CO_2 and H_2O, and the heat needed to raise the temperature of sorbent material and adsorbed species. The heat capacities of adsorbed CO_2 and H_2O were approximated using the pure component heat capacities of gaseous CO_2 and liquid H_2O, respectively. Parasitic losses such as pressure drops, heat losses, and heat transfer irreversibility were not considered. The modelling parameters for the DAC cycle are shown in Table 1.

The energy demands for sorbent regeneration in a TVSA process encompass the electrical input required for operating the vacuum pump,

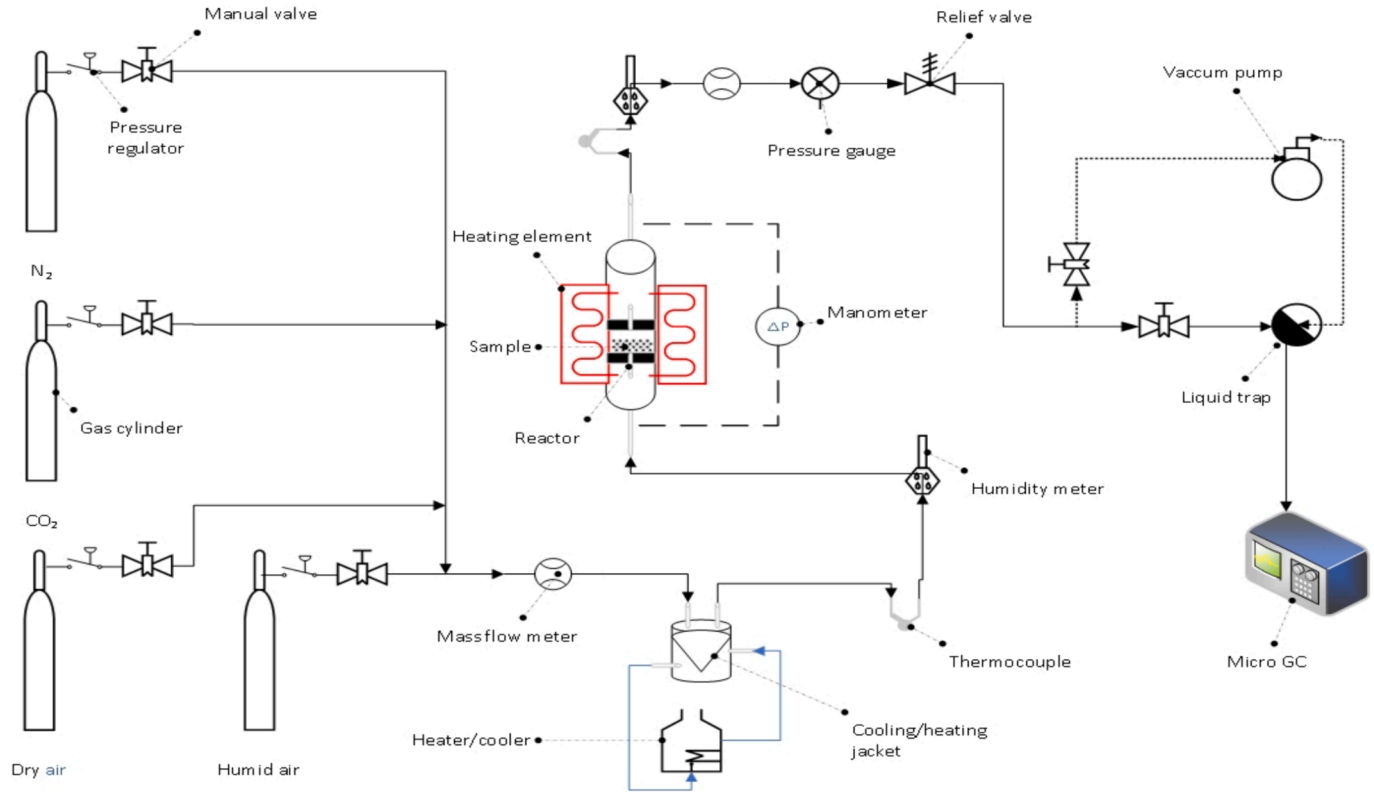

Fig. 1. Lab setup diagram for analyzing filter material performance under DAC conditions.

Table 1
The modelling parameters for the DAC cycle.

Parameter	Symbol	Value
Adsorption pressure (Pa)	P_{ads}	101,325
Adsorption CO_2 partial pressure (Pa)	$P_{partial,ads}$	42.556
Desorption pressure (Pa)	P_{des}	25,000
Partial pressure of CO_2 in treated air (Pa)	$P_{partial,treated}$	2.027
Desorption temperature (°C)	T_{des}	90
Isentropic efficiency (%)	η_{pump}	70
CO_2 recovery	Re_{CO2}	95 %
Pump temperature (K)	T_{pump}	350

expressed in kJ/mol CO_2 and calculated employing equation (1):

$$W_{vaccum} = \frac{R \cdot T_{pump}}{\eta_{pump}} . \ln\left(\frac{P_{amb}}{P_{des}}\right) \quad (1)$$

where W_{vaccum} is the compression energy and P_{amb} is the ambient pressure. The heat input for reaching the desorption temperature of the sorbent material, denoted as specific sensible heat in kJ/mol CO_2, is computed using equation (2):

$$Q_{sens} = \left(\frac{c_{p_{sorb}}}{\Delta q_{CO2}} + c_{p_{CO2}} + c_{p_{H2O}}\left(\frac{\Delta q_{H2O}}{\Delta q_{CO2}}\right)\right).(T_{des} - T_{ads}) \quad (2)$$

The CO_2 and H_2O working capacity of each material was measured exprimentally using the dynamic adsorption and desorption cycles with the details mentioned in the section of adsorption expriment. The specific heats of Lewatit and SBA-15 were obtained from experimental measurements in references [32,33] and [32,33]. Additionally, the required energy for cooling the regenerated adsorbent is determined via equation (3):

$$Q_L = \frac{c_{p_{sorb}}}{\Delta q_{CO2}} . (T_{des} - T_{ads}) \quad (3)$$

The heat input corresponding to the desorption enthalpies of CO_2 and H_2O, in kJ/mol CO_2, is calculated based on equation (4):

$$Q_{des} = \Delta H_{H2O}\left(\frac{\Delta q_{H2O}}{\Delta q_{CO2}}\right) + \Delta H_{CO2} \quad (4)$$

The heat of adsorption in case of dry conditions can be taken from Clausius–Clapeyron based on pure components adsorption relation for Lewatit [32] while in humid conditions it was taken from reference [34] which was calculated based on co-adsorption isotherms. The heat of adsorption for CO_2 on TEPA under dry conditions has been documented to predominantly involve carbamate reactions. This unique characteristic permits the utilization of its corresponding heat of reaction values in conjunction with the physical adsorption of CO_2, as deduced from Density Functional Theory (DFT) calculations. Under humid conditions, both carbamate and bicarbonate reactions were identified through FT-IR spectroscopy. The spectra notably revealed a higher bicarbonate formation in comparison to carbamate, particularly evident at a 15 % water content in the CO_2 stream [35]. It was elucidated that the mechanism governing the CO_2 reaction with TEPA is influenced by the probability of exposure, posing challenges in precisely quantifying the formation of each reaction. To facilitate comparison and maintain simplicity, this paper adopts the assumption that the bicarbonate reaction exclusively dominates. However, the heat of reaction values for S-TEP, S-PEI-L, and S-PEI-H used in this study were sourced from the literature based on experimental values, as referenced in Table 2.

Based on the information in Table 2 and to establish a clear comparison, it is assumed that the heat of adsorption for water on Lewatit, S-PEI-L, S-PEI-H and S-TEP is approximately 44.2 kJ/mol. This assumption is derived from the calculation of the average heat of adsorption (Q_{st}) when the water adsorption capacity falls within the range of 2.8–13.9 mmol/g. The consistency of Q_{st} across this range suggests a similar heat of adsorption for water on these materials. It's noteworthy

Table 2
The main parameters used to calculate the regeneration energy.

Material	Parameter	Calculation method	Value	Ref
Lewatit	Cp	DSC measurements	1.58 (kJ/kg. K)	[32]
	ΔH_{H2O}	Clausius–Clapeyron equation	−44.2 (kJ/mol)	[32]
	ΔH_{CO2}	Clausius–Clapeyron equation	−70 (kJ/mol)	[32]
S-TEP	C_p	DSC measurements	1.08 (kJ/kg. K)	[33]
	ΔH_{H2O}	Clausius–Clapeyron equation	−44.2 (kJ/mol)	[34]
	ΔH_{CO2}	DSC measurments	−104 (kJ/mol)	[22]
S-PEI-L	Cp	DSC measurements	1.08 (kJ/kg. K)	[33]
	ΔH_{H2O}	Clausius–Clapeyron equation	−44.2 (kJ/mol)	[34]
	ΔH_{CO2}	Combined calorimetric-volumetric adsorption	−93 (kJ/mol)	[36]
S-PEI-H	C_p	DSC measurements	1.08 (kJ/kg. K)	[33]
	ΔH_{H2O}	Clausius–Clapeyron equation	−44.2(kJ/mol)	[34]
	ΔH_{CO2}	DSC measurements	−83 (kJ/mol)	[37]

that the calculated value of 44.2 kJ/mol closely aligns with the vaporization heat of water. Additionally, the observation that Q_{st} remains relatively constant with increasing water adsorption capacity indicates the prevalence of a multilayer physisorption mechanism for water on each of these sorbent materials. The main Parameters used to calculate the regeneration energy and their calculated methods are presents in Table 2.

The overall heat requirement in kJ/mole of CO_2 separated is then derived using equation (5):

$$Q_{Total} = Q_{des} + Q_{sens} + Q_L \quad (5)$$

$$\eta_{TVSA} = \frac{Wmin}{W_{comp} + Q_H\left(1 - \frac{T_0}{T_H}\right) - Q_L\left(1 - \frac{T_0}{T_L}\right)} \quad (6)$$

Furthermore, equation (6) calculates the second-law efficiency of TVSA (ηTVSA) in practical processes, where the heat source temperature (T_H) is equivalent to the desorption temperature (T_{des}). Q_L represents the heat required for cooling the adsorbent, while Q_H denotes the input heat per cycle. The designated low temperature for cooling (T_L) is assumed to align with the ambient temperature as outlined in the cycle description. The reference or ambient temperature (T_0) is specifically defined as 298 K in this analysis. The minimum separation work was calculated based on equation (7):

$$W_{min} = -(R) \times T0 \times \left(ln\left(\frac{P_{partial,ads}}{P0}\right) - \left(1 - \left(\frac{P_{partial,ads}}{P0}\right)\right) \times \left(\frac{P_{partial,treated}}{P_{partial,ads} - P_{partial,treated}}\right) \times ln\left(\frac{P_{partial,treated}}{P_{partial,ads}}\right) + \left(1 - \left(\frac{P_{partial,ads}}{P0}\right)\right) \times \left(1 - \left(\frac{P_{partial,treated}}{P0}\right)\right) \times \left(\frac{P0}{P_{partial,ads} - P_{partial,treated}}\right) Ln\left(\frac{(P0 - P_{partial,ads})}{P0 - P_{partial,treated}}\right)\right) \quad (7)$$

The theoretical minimum energy of mixing represents the energy required for the complete separation of the input gas into pure CO_2 and CO_2-free air, with both streams delivered at ambient pressure, P_0. It is

essential to note that assuming complete removal of CO_2 from the air stream may not adequately account for partial removal. In a more general scenario represented by equation (7), the input stream, defined by a total pressure P_0 and a partial CO_2 pressure P_1, undergoes separation into a pure CO_2 stream and an air stream with a reduced CO_2 partial pressure ($P_2 < P_1$). Both input and output streams maintain a temperature T and total pressure P_0.

3. Results and discussions

3.1. Material characterization

Adsorbents have been developed through wet impregnation and chemical grafting approach, and subsequently have been subjected to various characterization techniques to confirm the successful functionalization of SBA-15 with different amine-functionalized precursors. Fig. 2 (a & b) show the N_2 isotherms at 77 K in the relative pressure range of 10^{-4} to 0.99. The isotherm for SBA-15 revealed type-IV isotherm with H_1 hysteresis loops, and its surface area and total pore volume were estimated to be 490 m^2/g and 1.17 cc/g, respectively. After functionalization as expected, the developed materials demonstrated a significantly low surface area (S-APT: 2.8 m^2/g, S-TEP: 41 m^2/g, S-PEI-L: 9 m^2/g and S-PEI-H: 54 m^2/g) and total pore volume S-APT: 0.01 cc/g, S-TEP: 0.14 cc/g, S-PEI-L: 0.04 cc/g and S-PEI-H: 0.18 cc/g) compared to SBA-15. The enlarged view of isotherms shown in Fig. 2(b) shows that the majority of the pores of SBA-15 were filled after functionalization with TEPA and PEI-L. The pore size distribution plots shown in Fig. 2(c) indicate that functionalized materials possess the mesoporous characteristics similar to SBA-15 except S-PEI-L. Interestingly, the pore size distribution for S-APT shows the peak at the mesopore region but a very low pore volume (0.01 cc/g), indicating that such pores are very small in number. The absence of any pore size distribution peak for S-PEI-L suggests that all the pores are filled.

Further, microstructural analysis using FE-SEM was carried out, as shown in Fig. 3. A smooth surface with open channels was observed for SBA-15 [Fig. 3(a)], whereas a significant change in surface microstructure can be observed upon functionalization [Fig. 3(b-e)]. After loading with TEPA and PEIs, the channels were not visible, indicating that the TEPA and PEIs were functionalized on the surface and pores of SBA-15. With APTES functionalization, channel walls became thicker, indicating the chemical grafting of APTES in the pore walls of SBA-15. FT-IR spectra, shown in Fig. 3(f), also supports the functionalization of SBA-15. The FT-IR spectrum for SBA-15 shows peaks at 1086 and 806 cm^{-1}, which are ascribed to asymmetric and symmetric stretching vibrations of Si-O-Si bonds, respectively [38]. After functionalization, new peaks at ~ 3300, 2900, 1590, 1470 and 1315 cm^{-1} were observed. The peaks at ~ 3300 and 1590 cm^{-1} are due to N–H stretching and bending vibrations, respectively [39]. The peak due to C-N stretching is observed at 1315 cm^{-1} [39], whereas stretching and bending vibrations for C–H bonds are observed at 2900 and 1470 cm^{-1}, respectively [40]. These results confirm the functionalization of SBA-15 with different amine-functionalized precursors.

The chemical nature of the adsorbents dictates the application properties, and elemental composition is a major driving factor in determining the chemical characteristics [41].To this end, elemental analysis was carried out using EDS (see Figures S1-S5). The detailed atomic compositions of the investigated samples are given in Table S1. The main constituents in SBA-15 are Si (40 %) and O (60 %), and as expected the percentage atomic composition for Si and O decreased upon functionalization. As the developed adsorbent are exclusively targeted for application in DAC, this is mostly influenced by the amount of amine functionality (N content) [40]. The amounts of N in S-APT, S-PEI-L, S-PEI-H and S-TEP were estimated to be 12, 11, 16 and 19 % (atomic), respectively. Furthermore, the presence of these elements was confirmed by XPS analysis. The XPS survey scan shows the additional peaks for C and N in S-APT, S-PEI-L, S-PEI-H and S-TEP compared to SBA-15 which has only Si and O peaks, as shown in Fig. 4(a). To further investigate the chemical nature of constituent elements, high-resolution XPS scans of individual elements were recorded and deconvoluted (Figure S6). The C1s XPS scan for S-APT shows four signals, attributed to carbon associated with C-Si, C–C, C-N, and C-O.[42] In S-TEP, S-PEI-L, and S-PEI-H, only one signal for carbon is observed, which may be ascribed to C attached with amine.[43] The N1s scan for S-APT reveals two signals due to nitrogen associated with $C\text{-}NH_2$ and $C\text{-}NH_3^+$.[44] Two N1s signal observed in S-TEP can be assigned to N associated with $C\text{-}NH_2$ and C-NH-C, however, three N1s signals observed in S-PEI-L and S-PEI-H are associated with primary, secondary, and tertiary amines.[45] The O1s scan for S-TEP, S-PEI-L, and S-PEI-H shows only one signal due to oxygen in Si-O-Si.[46] In S-APT, three signals for O1s were observed, and these can be ascribed to Si-O–H, Si-O-Si, and C-Si-O- linkages. [46,47] The Si2p scan for S-TEP, S-PEI-L, and S-PEI-H shows only one signal associated with Si-O-Si, while for S-APT exhibits two signals due to the presence of Si-O-Si and Si-O–H/C-Si-O linkages. [46,47].

TGA was performed to check the thermal stability of the materials, Fig. 4(b). For all the developed materials and SBA-15, a weight loss around 100 °C was observed which is mainly due to the adsorbed moisture and atmospheric gases, and solvents used for functionalization [48]. However, the mass loss due to moisture was more prominent for amine-functionalized samples compared to SBA-15, indicating the higher water affinity of these materials. As expected, there was no further mass loss step in SBA-15 up to 700 °C; however, S-APT, S-PEI-L, S-PEI-H and S-TEP demonstrated the mass loss step at different temperatures depending on the chemical nature of functionalizing group [49]. In S-APT, the APTES is chemically grafted in SBA-15, hence it shows higher thermal stability compared to S-PEI-L, S-PEI-H and S-TEP, in which the functionalization occurs through physical interactions. The weight loss steps around 300 °C in S-PEI-L, S-PEI-H and S-APT are attributed to the decomposition of organic amines. The amine decomposition step in S-TEP was observed at 180 °C and it could be due to the small size of TEPA compared to PEIs.

3.2. CO_2 adsorption performance

3.2.1. CO_2 adsorption isotherm

The atmospheric CO_2 concentration stands at approximately 400 ppm, equivalent to a partial pressure of 0.4 mbar in the mixed gas. Fig. 5

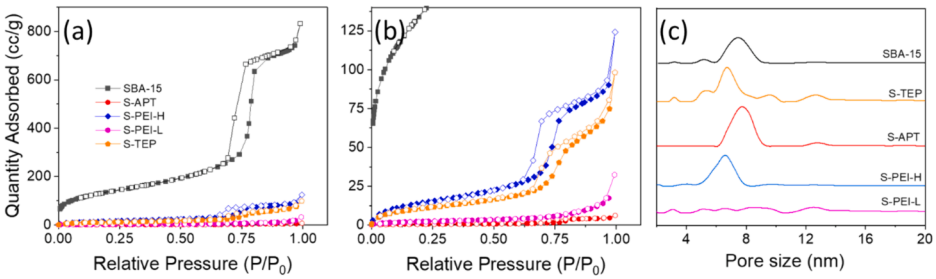

Fig. 2. N_2 sorption analysis: (a) N_2 isotherms (b) enlarged view of N_2 isotherm and (c) pore size distribution plots for SBA-15, S-APT, S-TEP, S-PEI-L and S-PEI-H.

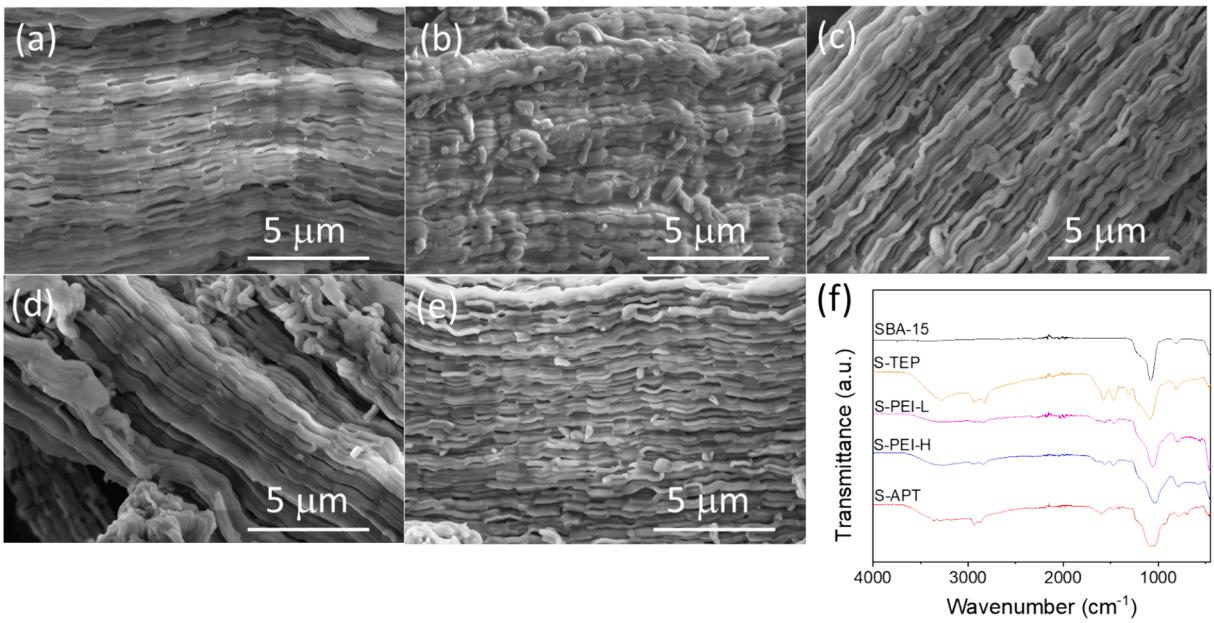

Fig. 3. FE-SEM images (a) SBA-15, (b) S-TEP, (c) S-PEI-L, (d) S-PEI-H, and (e) S-APT. (f) shows the FT-IR spectra.

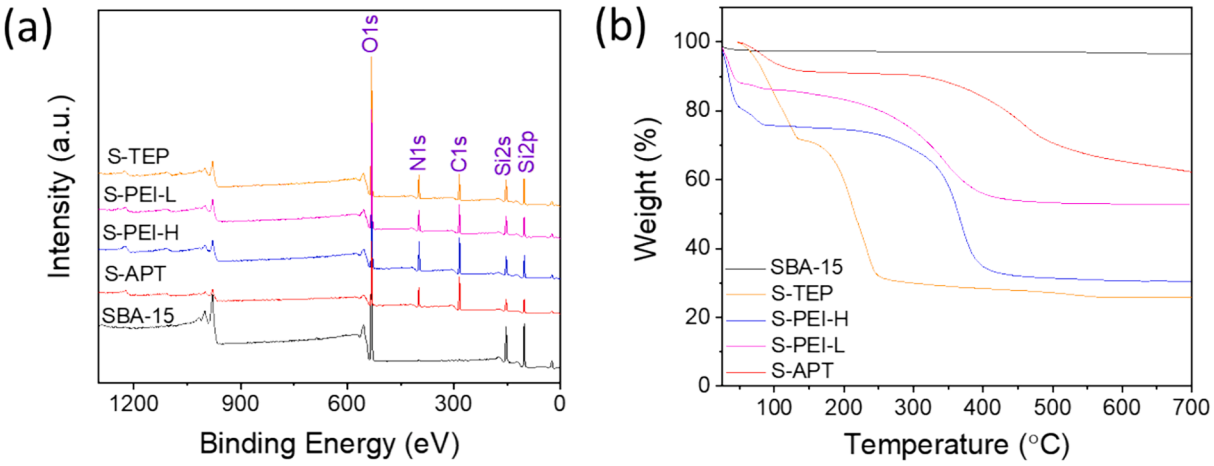

Fig. 4. (a) XPS survey scan and (b) TGA plots for SBA-15, S-TEP, S-APT, S-PEI-L and S-PEI-H.

illustrates CO_2 adsorption isotherms for SBA-15, S-APT, S-TEP, S-PEI-L, and S-PEI-H at room temperature (21 °C). The maximum uptake of 0.3 mmol/g at 1.0 bar was observed for SBA-15, while the uptake was negligible at low pressure. Interestingly, S-TEP, S-PEI-L, and S-PEI-H show a steep rise in uptake at very low pressure, and these adsorbents attain their maximum saturation adsorption capacity at a very low pressure, indicating strong binding energetics between adsorbates and adsorbents due to the presence of amine functional groups in significantly high density [50].Among all the adsorbents, the maximum uptake capacity of 2.5 mmol/g was observed for S-TEP, followed by S-PEI-L (1.5 mmol/g) and S-PEI-H (0.5 mmol/g). The uptake for S-APT was very low (0.07 mmol/g) even though its N content was 12 % (higher than S-PEI-L). This may be due to complete pore filling because of high APTES amount (50 %), and the amine functionality in the pores are inaccessible for binding with CO_2; hence, negligible CO_2 uptake was observed. The superior uptake observed for S-TEP is attributed to its highest nitrogen content (19 %) and better mass transfer rate due to its mesoporous characteristics. Although S-PEI-H shares a similar pore characteristic (mesoporous) and has a higher nitrogen content than S-PEI-L, its CO_2 uptake capacity is lower. This disparity may be attributed to the lower solubility of PEI-H because of very long chain, leading to agglomeration and significant deposition of amine on silica surface [51]. Consequently, a significant amount of the amine functional groups in S-PEI-H remains inaccessible for CO_2 binding, resulting in a lower CO_2 uptake capacity. It should be mentioned here that further adsorption experiments were carried out using three adsorbents: S-TEP, S-PEI-L, and S-PEI-H. The exclusion of pure SBA-15 and S-APT was based on their negligible adsorption capacity under the tested range of pressure and temperature.

3.2.2. CO_2 adsorption capacity under dynamic flow in dry conditions

In a fixed bed reactor with air flow rate of 35 ml/min, temperature of 21 °C, 420 ppm CO_2 and dry conditions, the adsorption capacities of three distinct materials, S-PEI-L, S-PEI-H and S-TEP, were evaluated as depicted in Fig. 6. Fig. 6(a) illustrates the dynamic changes in CO_2 concentration at the reactor outlet over a period of 1200 min. Specifically, S-TEP demonstrated the highest adsorption capacity, reaching 2.2 mmol/g and achieving saturation after 500 min, followed by S-PEI-L and S-PEI-H that reached maximum adsorption capacities of 1.2 and 1.0 mmol/g, respectively, with S-PEI-L reaching saturation at 400 min and S-PEI-H at 500 min. To gain a better understanding of the adsorption

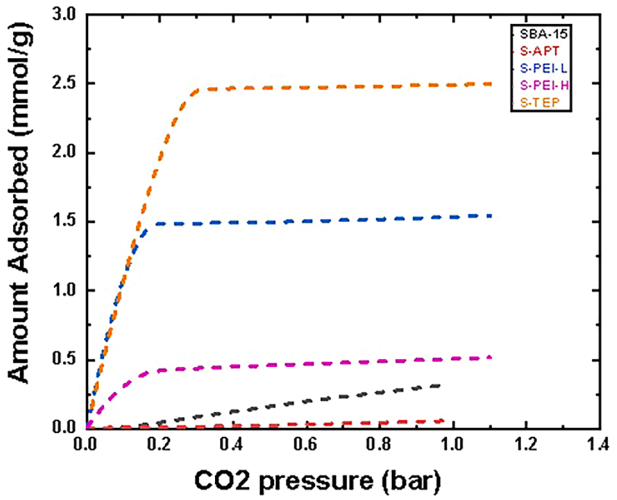

Fig. 5. CO_2 adsorption isotherms at 21 °C for SBA-15, S-APT, S-TEP, S-PEI-L, and S-PEI-H.

processes across these materials, kinetic models were applied, specifically employing PFO and Avrami Models, to fit the adsorption curves (Table 3). S-TEP demonstrated an adsorption half-time of 208.6 min and an equilibrium adsorption capacity of 2.16 mmol/g. This superior performance is attributed to its greater CO_2 adsorption capacity compared to S-PEIs, fostering a robust reaction between TEPA and CO_2, potentially influenced by the high nitrogen content in TEPA, as revealed by EDS data. Conversely, S-PEI-L exhibited an equilibrium adsorption capacity of 1.38 mmol/g, while S-PEI-H displayed the lowest adsorption capacity, necessitating adsorption half-times of 235 and 260 min, respectively.

adsorbents under dry conditions (T = 25 °C and P = 1 atm.): (a) adsorption (b) desorption.

The PEI's molecular weight affected the CO_2 uptake capacity as the higher molecular weight leads to a lower uptake capacity as shown in Fig. 6. The challenges associated with PEI-H, including high viscosity and thenanoporous nature of the support with some small pores reaching 2-3 nm, may lead to certain PEI-H molecules proving too large to infiltrate the material's such pores, causing agglomeration and pore blockage. This could explain the better performance of S-PEI-L compared to S-PEI-H. In summary, our comprehensive investigation into the kinetics of CO_2 adsorption using these materials, as detailed in Table 3, revealed comparable rate constants ranging from 0.00305 to 0.00434 min^{-1}. Additionally, the uniform value obtained for the coefficient of determination (R^2) reflects the high accuracy of the kinetic models in describing the adsorption behavior across these materials.

3.2.3. CO_2 adsorption capacity under dynamic flow in humid conditions

In order to have comparison between the adsorption capacity between dry and humid conditions, the adsorption performance of three adsorbents was evaluated under humid conditions, with a humidity level of 50 %. It should be mentioned that the 50 % RH was selected as it represents typical indoor atmospheric conditions. In parallel with the results obtained under dry conditions, S-TEP exhibited the highest adsorption capacity, reaching 3.3 mmol/g. S-PEI-L followed with an adsorption capacity of 2.5 mmol/g, while S-PEI-H displayed the lowest adsorption capacity of 1.7 mmol/g (Fig. 7). Notably, all adsorbents demonstrated an improvement in adsorption capacity under humid conditions. This enhancement in adsorption capacity can be attributed to the presence of amine groups, which exhibit increased CO_2 adsorption in the presence of water. The increased humidity facilitates a more favorable environment for the interaction between amine groups and CO_2 molecules, resulting in improved adsorption performance across all tested adsorbents. Jones et al. [52] conducted experiments on CO_2 adsorption using alkyl-aryl amine-rich small molecules in SBA-15 silica under both dry and humid conditions. Their study, focusing on ethylenediamine and propylenediamine revealed that the adsorption capacity under 30 % relative humidity conditions was found to be double that observed in dry conditions.

Given the intuitive impact of water on adsorption capacity, an in-depth analysis was conducted to examine the changes in capacity in its presence. The resulting curves were meticulously fitted to both PFO and Avrami models as shown in Fig. 7 and Table S2. It becomes evident that the complexity of the adsorption performance renders the PFO model inadequate for explaining the kinetics. Notably, a consistent shift in time is observed across all materials, indicating a prolonged duration for reaching equilibrium under humid conditions. The breakthrough curves for supported amines exhibit a rightward shift, suggesting a potential increase in capacity. Both the breakthrough time and the equilibrium time were longer. This could be a possible decrease in kinetics in the presence of water or the longer time could be interpreted by the higher CO_2 capacity which needs longer time to be saturated, unveiling a nuanced interplay between water content and the kinetic aspects of the

Table 3
The kinetic models of CO_2 adsorption fitted parameter under dry conditions.

Sample	Model	q_e(mmol/g)	k(min^{-1})	n	R^2
S-PEI-H	PFO	1.13687	0.00383	–	0.98082
S-PEI-L	PFO	1.38243	0.00417	–	0.98082
S-TEP	PFO	2.16174	0.00305	–	0.98082
S-PEI-H	Avrami	1.12767	0.00385	1.08612	0.99943
S-PEI-L	Avrami	1.33518	0.00434	1.40267	0.9982
S-TEP	Avrami	2.15777	0.00306	1.02808	0.94325

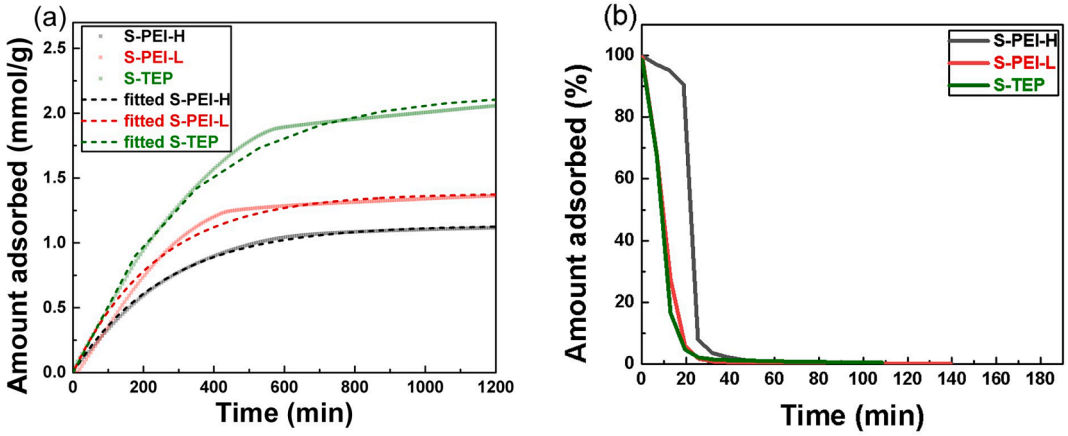

Fig. 6. The Adsorption curve rate and fitted kinetic model for CO_2 adsorption using three.

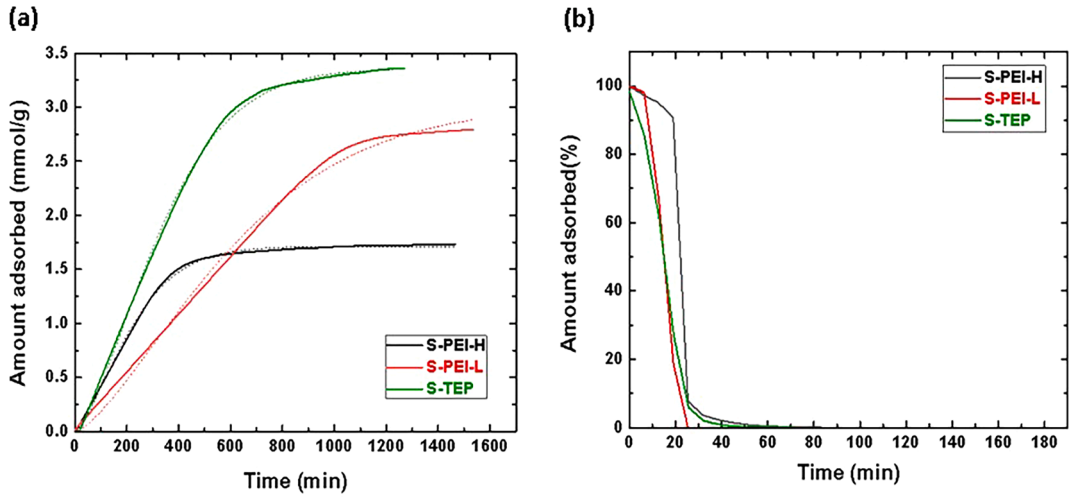

Fig. 7. The adsorption curve rate and fitted kinetic model for CO_2 adsorption using three adsorbents under 50 % humidity (T = 25 °C and P = 1 atm.): (a) adsorption (b) desorption.

adsorption process which needs further investigation. Clearly, the equilibrium adsorption capacities of 3.4 and 3.0 mmol/g obtained from the kinetic model for S-TEP and S-PEI-L, respectively, are comparable to their corresponding experimental values. However, S-PEI-L required a longer time to reach equilibrium (685 min) in contrast to S-PEI-H that required only 249 min to reach the maximum capacity of 1.7 mmol/g.

It should be mentioned that for physical adsorbents, the most common role of water is to result in competitive adsorption against CO_2, so CO_2 capacity is typically reduced under humid condition. For supported amines, instead of water competitive adsorption, the chemical reaction mechanism, which typically changes in humid gas, is more significant. Namely, the reaction of amines with CO_2 in the absence and presence of water produces ammonium carbamate and bicarbonate, respectively. The latter has a more favorable CO_2/amine equivalence ratio, so CO_2 capacity generally increases in humid gas.

3.3. Water adsorption and loading

The adsorption behavior of H_2O, as illustrated in Fig. 8, was systematically investigated using the DAC system under humid conditions (50 % RH) for three distinct adsorbents: S-PEI-H, S-PEI-L and S-TEP. It is noteworthy that the H_2O loading exhibited a notable dependence on the type of absorbent employed. For S-PEI-H, the H_2O capacity was measured at 4.4 mmol H_2O/g. Subsequently, the H_2O capacity increased significantly, reaching almost 10 mmol H_2O/g for S-PEI-L. This substantial augmentation in H_2O capacity is attributed to the enhanced adsorption performance of S-PEI-L, which is characterized by a greater number of amine active sites. This observation is consistent with the findings from CO_2 adsorption studies conducted under humid conditions.

Notably, S-TEP demonstrated the highest water loading, achieving a remarkable uptake capacity of 12 mmol/g. This underscores its superior adsorption capacity compared to S-PEI adsorbents The exceptional performance of S-TEP can be attributed to its higher density of active functional groups, more favorable pore structure and stronger chemical affinity for water molecules. Amine-functionalized adsorbents have exhibited minimal impact from CO_2 on H_2O equilibrium adsorption up to relative humidities of at least 60 %. Conversely, these studies have demonstrated a significant enhancement in CO_2 adsorption due to the presence of H_2O, emphasizing the need for a detailed understanding of the chemical mechanisms underlying the co-adsorption of CO_2 and H_2O on amine-functionalized sorbents. This study employs two models to elucidate the kinetics of water adsorption during CO_2 adsorption under humid conditions. Notably, the H_2O adsorption curves is effectively fitted to the Avrami model, and the parameters are shown in the Table S3. While various adsorption models have been employed to describe water adsorption isotherms, it is essential to recognize that no single adsorption mechanism universally applies to all amine-functionalized sorbents. Instead, multiple mechanisms may be at play on a single absorbent. This discussion briefly outlines three key mechanisms integral to deriving mechanistically consistent pure adsorption isotherm models for water loading: changes in amine efficiency (i.e.,

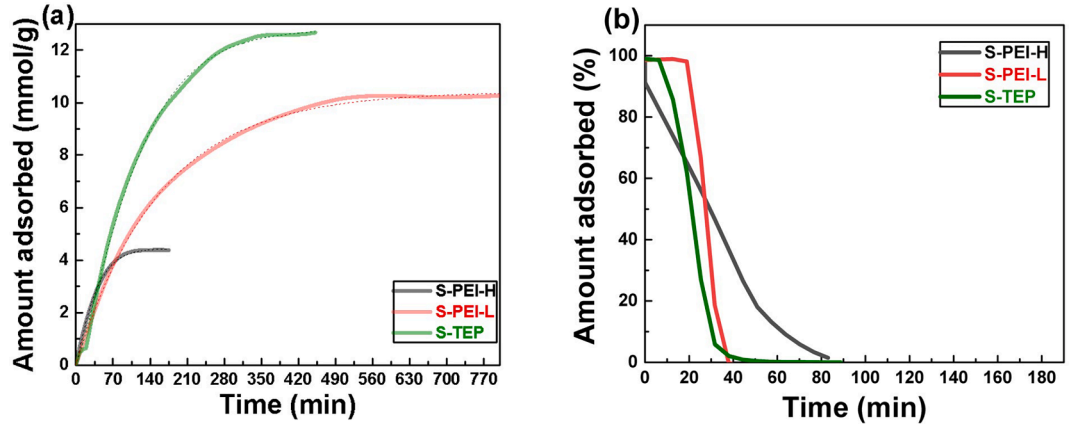

Fig. 8. The kinetics of water adsorption using three adsorbents (T = 25 °C and P = 1 atm.). (a) adsorption rate curves and (b) desorption rate curves.

CO_2 adsorption stoichiometry), alterations in the heat of adsorption impacting the sorbent's affinity to CO_2, and amine site blocking by adsorbed water molecules.

3.4. Thermodynamic efficiency and energy consumptions of adsorbents

This study conducted a comprehensive analysis of three adsorbents within a DAC system, focusing on their energy consumption and thermodynamic efficiency under both dry and humid conditions. Fig. 9(a) provides a detailed overview of thermal energy consumption and thermodynamic efficiency for various materials, revealing the intricate interplay between material properties and environmental conditions. Notably, the S-TEP material exhibits a significant increase in total thermal energy consumption from 174.8 to 327.7 kJ/mol_{CO2} when transitioning from dry to humid conditions. This rise in energy requirements is coupled with a notable reduction in thermodynamic efficiency, decreasing from 69.1 % to 35.5 %. The same effect of humidity was also noticed for the other materials as illustrated in Fig. 6. These findings underscore the material's sensitivity to humidity, emphasizing its impact on both performance and efficiency in thermal energy conversion processes.

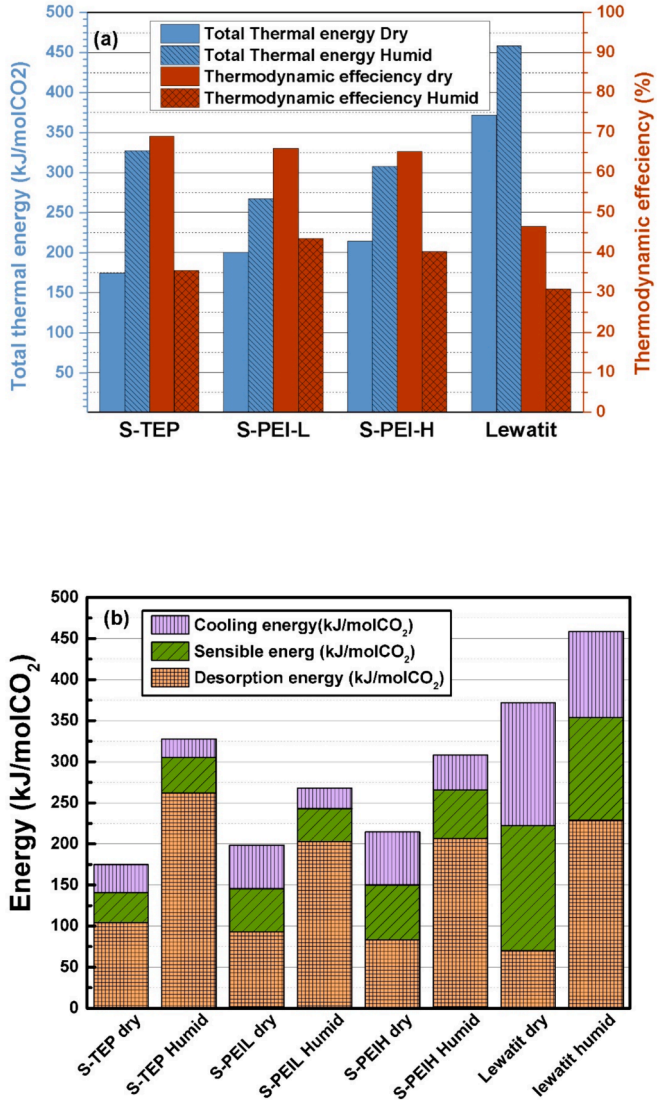

Fig. 9. (a) Thermodynamic efficiency and total thermal energy for several adsorbents under dry and wet conditions. (b) Total thermal energy consumption for the three adsorbents.

Exploring the influence of functionalization, a compelling comparison arises between S-TEP, and S-PEI-L and S-PEI-H. Under dry conditions, S-TEP demonstrates the highest efficiency at 69.1 %, surpassing both S-PEI-L (66 %) and S-PEI-H (65.3 %). This nuanced response underscores the intricate relationship between functionalization and environmental factors, emphasizing the need for careful consideration of these variables in material selection for optimal thermal energy conversion. While S-TEP exhibits the highest adsorption capacity under both dry and wet conditions, optimization for thermodynamic efficiency may be necessary for direct application in the presence of water. On the other hand, S-PEI-L demonstrates the highest efficiency and moderate adsorption capacity, making it a promising candidate for DAC system applications in humid environments.

Additionally, a comparative analysis with the common commercial adsorbent, Lewatit, provides valuable insights. Despite demonstrating higher total thermal energy consumption in both dry and humid conditions, Lewatit maintains less thermodynamic efficiency values (46.5 % and 30.9 %, respectively). Morever, it has a low adsorption capacity, reaching only 1 mmol/g under humid conditions[32], compared to S-TEP, S-PEI-L and S-PEI-H, which boast adsorption capacities of 3.17, 2.86 and 1.68 mmol/g under humid conditions, respectively. The contrasting performance of Lewatit and the SBA-15 variants highlights the diversity in material responses and their potential suitability for specific applications. In practical terms, these findings underscore the critical importance of tailoring material selection to the specific environmental conditions of a given application. Whether considering the sensitivity of SBA-15 variants to humidity or the nuanced performance of Lewatit, scientists must carefully account for these factors to optimize the efficiency of thermal energy conversion systems. Moreover, the data prompts further exploration into the molecular and structural changes within these materials in response to humidity, offering a promising avenue for future research aimed at refining material design for enhanced performance in diverse operating environments.

For the design and costing of DAC systems featuring amine-functionalized adsorbents, a comprehensive understanding of single-component and binary CO_2 and H_2O adsorption is crucial because the CO_2 output and energy requirement of the DAC system depend on the temperature and relative humidity of air. The total energy consumption of the adsorbent material is intricately linked to the desorption energy, a parameter that varies notably between dry and humid conditions. This distinction arises from the adsorption and desorption processes of water molecules within the material, which exert a direct influence on the adsorption energy. Specifically, the presence of water alters the interactions between the adsorbent surface and the target molecules, impacting both the adsorption and desorption energies. CO_2 adsorption in the presence of H_2O has been examined for concentrated sources and diluted sources, but little is known about co-adsorption of CO_2 and H_2O in a range of conditions relevant to DAC. In the overall context, desorption energy significantly governs total energy consumption, exerting a predominant influence over sensible and cooling energy. This is evident as desorption energy accounts for approximately 48 % to 63 % of the total thermal energy. However, nuances arise under specific conditions.

Under dry conditions, S-TEP, and S-PEI-L and S-PEI-H demonstrate desorption energy values of approximately 104, 93 and 83 kJ/mol CO_2 respectively. Notably, desorption energy tends to be higher in humid adsorption due to increased water co-adsorption, necessitating a higher amount of heat for desorbing water molecules. In the realm of energy dynamics, cooling energy is less for dry conditions compared to humid conditions. The variation in cooling energy among materials is attributed to their respective heat capacities and the amount of CO_2 captured, showcasing S-TEP's achievement of the minimum cooling energy owing to its highest CO_2 capacity. Furthermore, under dry conditions, S-TEP stands out by attaining the lowest thermal energy among all materials. While S-TEP, and S-PEI-L share close desorption energy values in dry conditions, S-TEP excels by achieving the lowest cooling and sensible

heating energy per mol for CO_2, courtesy of its superior capacity. In contrast, under humid conditions, S-PEI-L emerges with the minimum regeneration energy compared to other materials. This can be attributed to its low water co-adsorption aligning with moderate CO_2 adsorption, resulting in lower regeneration energy requirements. Fig. 9 (b) illustrates the pivotal role of CO_2 capacity in assessing adsorbent performance. Higher CO_2 capacity generally correlates with lower regeneration energy. However, it is crucial to consider additional factors such as water co-adsorption and adsorption enthalpy, which introduce variability in the energy trends. The selection of the optimal sorbent is further complicated by environmental conditions, emphasizing the importance of considering water co-adsorption effects in the decision-making process for both humid and dry scenarios.

3.5. Material stability

A critical aspect of adsorbents' efficiency in real-world applications is their exceptional adsorption capacity, rapid kinetics, and superior regenerability. The research examined the regenerability of S-TEP, S-PEI-L, S-PEI-H and Lewatit. Cyclic adsorption/desorption tests were conducted, maintaining adsorption conditions at 23 °C for 120 min with a 400 ppm CO_2 in N_2 flow of 100 mL/min, and desorption conditions at 90 °C for 90 min with a pure N_2 flow of 100 mL/min. The adsorbent material was tested for 10 adsorption/desorption cycles for a period of 40 h under dry condition and wet conditions.

It's important to note that material stability testing typically occurs under dry conditions, without humidity. However, for a comprehensive assessment of material stability in real-world applications, especially in indoor settings where conditions may involve humidity, further testing is necessary. To better evaluate the stability of the adsorbent, all materials were subjected to humid conditions (RH = 50 %), mimicking typical indoor DAC. The observed CO_2 and H_2O uptake capacities are illustrated in Fig. 10.

The data in Fig. 10 shows that all four materials—S-TEP, S-PEI-L, S-PEI-H, and Lewatit—maintain stable CO_2 uptake capacities under humid conditions across ten cycles. Notably, the CO_2 uptake capacity for all materials increased under humid conditions compared to dry conditions. Among these, S-TEP exhibits the highest CO_2 uptake capacity under humid conditions, reaching approximately 3.17 mmol/g, compared to its lower uptake of 2.1 under dry conditions. S-PEI-H and S-PEI-L also demonstrate increased performance under humid conditions, with capacities around 2.87 mmol/g and 1.68 mmol/g, respectively, compared to their dry condition performance. Lewatit, while showing the lowest CO_2 uptake capacity, also benefits from increased uptake under humid conditions, maintaining consistency at approximately 1 mmol/g.

Under humid conditions, the water uptake of the materials was also monitored. S-TEP again showed the highest water uptake capacity, nearing 11.34 mmol/g. In contrast, Lewatit displayed the lowest water uptake capacity at around 3.58 mmol/g. Both S-PEI-L and S-PEI-H showed stable water uptake capacities, with values fluctuating around 4–5 mmol/g and 7–8 mmol/g, respectively. However, it is important to note that higher water uptake can be detrimental to DAC applications as it leads to higher regeneration energy requirements. Therefore, there is a balance between CO_2 and water uptake; while higher water uptake generally correlates with increased CO_2 uptake, it also means more

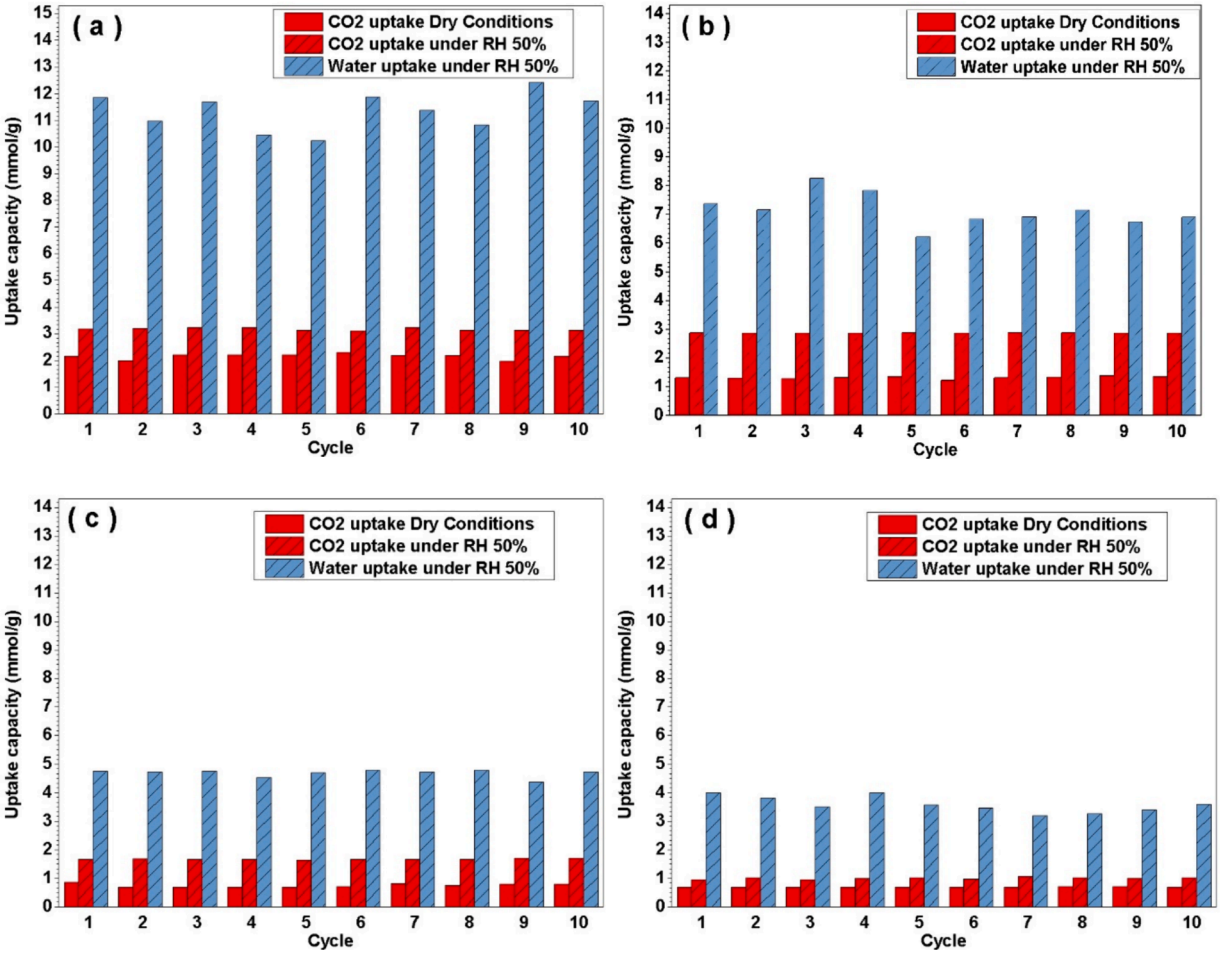

Fig. 10. The cyclic CO_2 adsorption capacity for (a) S-TEP (b) S-PEI-L (c) S-PEI-H (d) Lewatit, adsorption at 23 °C and degassing at 90 °C under dry and humid conditions.

energy is needed for regeneration. This analysis underscores the potential of S-TEP, S-PEI-L, and S-PEI-H to compete effectively with Lewatit, offering higher CO_2 and water uptake capacities under real-world conditions, while also considering the trade-off between CO_2 capture efficiency and energy costs for regeneration.

4. Conclusions

This research investigated the CO_2 adsorption performance of SBA-15 functionalized with TEPA, PEI-L, PEI-H, and APTES in the context of DAC application, considering humidity levels. Functionalization led to substantial improvements in CO_2 adsorption capacities: S-TEP, S-PEI-L and S-PEI-H exhibited capacities of 2.1, 1.36, and 1.11 mmol/g, respectively. Humidity further increased the CO_2 uptake capacities to 3.17, 2.87, and 1.68 mmol/g. However, this enhancement came at a thermodynamic efficiency trade-off, with efficiency decreasing from 69 %, 66 %, and 65 % to 36 %, 44 %, and 40 % in dry conditions. S-TEP demonstrated the highest efficiency of 69 % in dry conditions, while S-PEI-L achieved the highest efficiency of 44 % in humid conditions. The stability test of the S-TEP, S-PEI-L, S-PEI-H and lewatit demonstrates robust regenerability over 10 cycles, under both dry and humid conditions, with stable performance despite moderate adsorption uptake. This study provides crucial insights into the interplay between functionalization, humidity, and thermodynamic efficiency in CO_2 adsorption, offering promising avenues for the development of efficient and sustainable DAC processes and for the application in the indoor DAC application.

CRediT authorship contribution statement

Riham Surkatti: Writing – original draft, Software, Methodology, Investigation, Formal analysis, Data curation, Conceptualization. **Yasser M. Abdullatif:** Writing – original draft, Visualization, Validation, Software, Methodology, Investigation, Formal analysis, Data curation, Conceptualization. **Raeesh Muhammad:** Writing – original draft, Visualization, Validation, Methodology, Investigation, Formal analysis, Data curation, Conceptualization. **Ahmed Sodiq:** Writing – review & editing, Methodology, Investigation, Conceptualization. **Kamal Mroue:** Writing – review & editing, Investigation, Data curation, Conceptualization. **Tareq Al-Ansari:** Writing – review & editing, Resources, Methodology, Investigation, Funding acquisition, Conceptualization. **Abdulkarem I. Amhamed:** Writing – review & editing, Project administration, Methodology, Investigation, Funding acquisition, Conceptualization.

Declaration of competing interest

The authors declare that they have no known competing financial interests or personal relationships that could have appeared to influence the work reported in this paper.

Data availability

Data will be made available on request.

Acknowledgements

Authors acknowledge the financial support from Qatar Environment and Energy Research institute (QEERI), Hamad bin Khalifa University (HBKU) (member of Qatar Foundation). The authors also would like to acknowledge the Core Labs, Hamad Bin Khalifa University and Dr. Said A. Mansour for their contribution in the material characterization. This publication was made possible by NPRP 12 grant # (NPRP12C-0821-190017), GSRA8-L-1-0506-21032 from the Qatar National Research Fund (a member of the Qatar Foundation). The findings herein reflect the work and are solely the responsibility of the authors. Open Access funding provided by the Qatar National Library.

Appendix A. Supplementary material

Supplementary data to this article can be found online at https://doi.org/10.1016/j.seppur.2024.128641.

References

[1] C. Lv, et al., Selective electrocatalytic synthesis of urea with nitrate and carbon dioxide, Nat. Sustainability 4 (10) (2021) 868–876.
[2] G.P. Peters, et al., Carbon dioxide emissions continue to grow amidst slowly emerging climate policies, Nat. Clim. Chang. 10 (1) (2020) 3–6.
[3] L. Lu, et al., Wastewater treatment for carbon capture and utilization, Nat. Sustainability 1 (12) (2018) 750–758.
[4] C. Bettenhausen, The case for direct air capture, C&EN Global Enterprise 100 (2022) 22–24.
[5] H.O. Pörtner, et al., Climate change 2022: impacts, adaptation and vulnerability, IPCC, 2022.
[6] D. Goldberg, K. Lackner, Creating negative emissions at remote CO2 sequestration sites, Greenhouse Gases Sci. Technol. 5 (3) (2015) 238–240.
[7] Lackner, K.S., et al., *The urgency of the development of CO2 capture from ambient air*. Proceedings of the National Academy of Sciences, 2012. **109**(33): p. 13156-13162.
[8] K.S. Lackner, A guide to CO2 sequestration, Science 300 (5626) (2003) 1677–1678.
[9] E.S. Sanz-Pérez, et al., Direct capture of CO2 from ambient air, Chem. Rev. 116 (19) (2016) 11840–11876.
[10] F. Bisotti, et al., Direct air capture (DAC) deployment: National context cannot be neglected. A case study applied to Norway, Chem. Eng. Sci. 282 (2023) 119313.
[11] T. Terlouw, et al., Life cycle assessment of direct air carbon capture and storage with low-carbon energy sources, Environ. Sci. Tech. 55 (16) (2021) 11397–11411.
[12] A.R. Sujan, et al., Direct CO2 capture from air using poly (ethylenimine)-loaded polymer/silica fiber sorbents, ACS Sustain. Chem. Eng. 7 (5) (2019) 5264–5273.
[13] A. Sayari, Y. Belmabkhout, Stabilization of amine-containing CO2 adsorbents: dramatic effect of water vapor, J. Am. Chem. Soc. 132 (18) (2010) 6312–6314.
[14] J.A. Wurzbacher, C. Gebald, A. Steinfeld, Separation of CO2 from air by temperature-vacuum swing adsorption using diamine-functionalized silica gel, Energ. Environ. Sci. 4 (9) (2011) 3584–3592.
[15] O. Akingbogun, L. Muhr, C. Vallieres, Capture of carbon dioxide by an ion-exchange resin: Influence of gas humidity on capture mechanisms, Sep. Sci. Technol. 52 (10) (2017) 1761–1767.
[16] W.C. Wilfong, B.W. Kail, M.L. Gray, Rapid screening of immobilized amine CO2 sorbents for steam stability by their direct contact with liquid H2O, ChemSusChem 8 (12) (2015) 2041–2045.
[17] K.S. Sánchez-Zambrano, et al., CO2 capture with mesoporous silicas modified with amines by double functionalization: Assessment of adsorption/desorption cycles, Materials 11 (6) (2018) 887.
[18] A.R. Sujan, et al., Poly (glycidyl amine)-loaded SBA-15 sorbents for CO2 capture from dilute and ultradilute gas mixtures, ACS Applied Polymer Materials 1 (11) (2019) 3137–3147.
[19] Y. Miao, et al., Operating temperatures affect direct air capture of CO2 in polyamine-loaded mesoporous silica, Chem. Eng. J. 426 (2021) 131875.
[20] J.-T. Anyanwu, Y. Wang, R.T. Yang, SBA-15 Functionalized with Amines in the Presence of Water: Applications to CO2 Capture and Natural Gas Desulfurization, Ind. Eng. Chem. Res. 60 (17) (2021) 6277–6286.
[21] D.R. Kumar, et al., Alkyl-Aryl Amine-Rich Molecules for CO2 Removal via Direct Air Capture, ACS Sustain. Chem. Eng. 8 (29) (2020) 10971–10982.
[22] V. Kulkarni, D. Panda, S.K. Singh, Direct Air Capture of CO2 over Amine-Modified Hierarchical Silica, Ind. Eng. Chem. Res. 62 (8) (2023) 3800–3811.
[23] D. Wang, X. Wang, C. Song, Comparative Study of Molecular Basket Sorbents Consisting of Polyallylamine and Polyethylenimine Functionalized SBA-15 for CO2 Capture from Flue Gas, ChemPhysChem 18 (22) (2017) 3163–3173.
[24] A. Holewinski, M.A. Sakwa-Novak, C.W. Jones, Linking CO2 Sorption Performance to Polymer Morphology in Aminopolymer/Silica Composites through Neutron Scattering, J. Am. Chem. Soc. 137 (36) (2015) 11749–11759.
[25] Y. Meng, et al., Comprehensive study of CO2 capture performance under a wide temperature range using polyethyleneimine-modified adsorbents, J. CO2 Util. 27 (2018) 89–98.
[26] G. Zhang, et al., Amine-modified SBA-15 (P): A promising adsorbent for CO2 capture, J. CO2 Util. 24 (2018) 22–33.
[27] M. Jahandar Lashaki, S. Khiavi, A. Sayari, Stability of amine-functionalized CO2 adsorbents: a multifaceted puzzle, Chem. Soc. Rev. 48 (12) (2019) 3320–3405.
[28] X. Duan, et al., Chemisorption and regeneration of amine-based CO2 sorbents in direct air capture, Materials Today Sustainability 23 (2023) 100453.
[29] J.M. Kolle, M. Fayaz, A. Sayari, Understanding the effect of water on CO2 adsorption, Chem. Rev. 121 (13) (2021) 7280–7345.
[30] C. Drechsler, D.W. Agar, Investigation of water co-adsorption on the energy balance of solid sorbent based direct air capture processes, Energy 192 (2020) 116587.
[31] J.A. Wurzbacher, et al., Concurrent Separation of CO2 and H2O from Air by a Temperature-Vacuum Swing Adsorption/Desorption Cycle, Environ. Sci. Tech. 46 (16) (2012) 9191–9198.

[32] J. Young, et al., The impact of binary water–CO2 isotherm models on the optimal performance of sorbent-based direct air capture processes, Energ. Environ. Sci. 14 (10) (2021) 5377–5394.
[33] E. Ghedini, et al., Multifunctional and Environmentally Friendly TiO2–SiO2 Mesoporous Materials for Sustainable Green Buildings, Molecules 24 (23) (2019) 4226.
[34] C. Xu, et al., Adsorption mechanisms and regeneration heat analysis of a solid amine sorbent during CO2 capture in wet flue gas, Energy 284 (2023) 129379.
[35] Y. Wang, et al., Mechanism and kinetics of CO2 adsorption for TEPA- impregnated hierarchical mesoporous carbon in the presence of water vapor, Powder Technol. 368 (2020) 227–236.
[36] M.E. Potter, S.H. Pang, C.W. Jones, Adsorption microcalorimetry of CO2 in confined aminopolymers, Langmuir 33 (1) (2017) 117–124.
[37] A. Goeppert, et al., Easily Regenerable Solid Adsorbents Based on Polyamines for Carbon Dioxide Capture from the Air, ChemSusChem 7 (5) (2014) 1386–1397.
[38] H. Dan, et al., Efficient adsorption of CO2 by amino-functionalized short pore SBA-15: Influence of pore length on adsorption capacity and amino efficiency, J. Environ. Chem. Eng. 11 (6) (2023) 111379.
[39] L. Lin, et al., Comparison of characteristics and performance between PEI and DETA impregnated on SBA-15 for CO2 capture, Sep. Purif. Technol. (2023) 124346.
[40] R. Muhammad, P. Mohanty, Nitrogen enriched triazine bridged mesoporous organosilicas for CO2 capture and dye adsorption applications, J. Mol. Liq. 248 (2017) 127–134.
[41] R. Muhammad, et al., Facile synthesis of ultrahigh-surface-area and hierarchically porous carbon for efficient capture and separation of CO2 and enhanced CH4 and H2 storage applications, Chem. Eng. J. 473 (2023) 145344.
[42] T. Zhang, et al., Modified Boron Nitride Nanosheets-Loaded Palladium Nanoparticles: An Air-Stable, Highly Active, and Recyclable Multiphase Catalyst for the Suzuki Reaction, Catal. Lett. 154 (1) (2024) 224–236.
[43] H. Park, et al., Laser-Assisted Direct Grafting of Poly (ethyleneimine) on Poly (methyl methacrylate), Polymers 14 (10) (2022) 2041.
[44] H. Hafeez, et al., Replacement of n-type layers with a non-toxic APTES interfacial layer to improve the performance of amorphous Si thin-film solar cells, RSC Adv. 9 (13) (2019) 7536–7542.
[45] H. He, et al., Preparation and properties of a hyperbranch-structured polyamine adsorbent for carbon dioxide capture, Sci. Rep. 7 (1) (2017) 3913.
[46] N. Paengjun, K. Vibulyaseak, M. Ogawa, Heterostructural transformation of mesoporous silica–titania hybrids, Sci. Rep. 11 (1) (2021) 3210.
[47] J. McKenna, et al., Synthesis and surface engineering of nanomaterials by atmospheric-pressure microplasmas, The European Physical Journal-Applied Physics 56 (2) (2011) 24020.
[48] H. Yan, et al., Amine-functionalized disordered hierarchical porous silica derived from blast furnace slag with high adsorption capability and cyclic stability for CO2 adsorption, Chem. Eng. J. (2023) 147480.
[49] H.J. Moon, J.M.Y. Carrillo, C.W. Jones, Distribution and Mobility of Amines Confined in Porous Silica Supports Assessed via Neutron Scattering, NMR, and MD Simulations: Impacts on CO2 Sorption Kinetics and Capacities, Acc. Chem. Res. 56 (19) (2023) 2620–2630.
[50] L. Zhang, et al., Impregnation of polyethylenimine in mesoporous multilamellar silica vesicles for CO2 capture: a kinetic study, Ind. Eng. Chem. Res. 55 (20) (2016) 5885–5891.
[51] A. Dindi, et al., Effect of PEI impregnation on the CO2 capture performance of activated fly ash, Energy Procedia 114 (2017) 2243–2251.
[52] G. Rim, et al., Sub-ambient temperature direct air capture of CO2 using amine-impregnated MIL-101 (Cr) enables ambient temperature CO2 recovery, Jacs Au 2 (2) (2022) 380–393.